Performance and environmental study of a biogas-fuelled solid oxide fuel cell with different reforming approaches

Narissara Chatrattanawet [a], Dang Saebea [b], Suthida Authayanun [c], Amornchai Arpornwichanop [d], Yaneeporn Patcharavorachot [a,*]

[a] Department of Chemical Engineering, Faculty of Engineering, King Mongkut's Institute of Technology Ladkrabang, Bangkok, 10520, Thailand
[b] Department of Chemical Engineering, Faculty of Engineering, Burapha University, Chonburi, 20131, Thailand
[c] Department of Chemical Engineering, Faculty of Engineering, Srinakharinwirot University, Nakhon Nayok, 26120, Thailand
[d] Computational Process Engineering Research Unit, Department of Chemical Engineering, Faculty of Engineering, Chulalongkorn University, Bangkok, 10330, Thailand

ARTICLE INFO

ABSTRACT

In this work, solid oxide fuel cells (SOFCs) using biogas as the fuel with two different reforming approaches, i.e., external and internal reforming, were studied to determine the optimal operation conditions for each approach. Thermodynamic analysis was performed using a flowsheet simulator. The equilibrium gas composition was calculated by minimizing the Gibbs free energy. An electrochemical model that includes three voltage losses (i.e., activation, ohmic, and concentration losses) was used to predict the performance of the SOFCs. The simulation results showed that the reformer in the external reforming SOFC should be operated at a temperature of 973 K, a pressure of 1 atm, and a steam-to-carbon molar ratio of 0.5. In performance analysis, the simulation results indicated that both approaches have the same optimal operating conditions, i.e. a temperature of 1173 K, a pressure of 3 atm, and a current density of 5000 A/m^2. Under the same operating conditions, the internal reforming SOFC exhibited better electrical efficiency than that of the external reforming SOFC. Considering the CO_2 and CO emissions, the exhaust gas obtained from the anode side of the internal reforming SOFC contained 7.4% CO_2 and 37.9% CO, which are higher values than those for the external reforming SOFC (1.9% CO_2 and 32.5% CO).

© 2017 Elsevier Ltd. All rights reserved.

1. Introduction

Increasing global energy consumption has led to the depletion of fossil fuels, which are used as fuel resources in power generation. In addition, the use of fossil fuels results in environmental problems such as global warming and climate change. As a result, many researchers are pursuing the development of new energy technologies that are more efficient and entail lower emission of pollutants to the environment. Fuel cell technology is an attractive option for the future, as the chemical energy contained in gaseous fuels can be directly converted into electricity via electrochemical reactions [1]. Compared with conventional methods for power generation, fuel cells are highly efficient and environmentally benign energy conversion devices because they can produce electricity without combustion [2]. Of the several types of fuel cell, solid oxide fuel cells (SOFCs) have attracted considerable interest owing to their high-temperature operation (1073–1273 K). The main advantage of the high-temperature operation of SOFCs is its compatibility with a variety of fuels, e.g., CH_4, ethanol, and biogas, due to the possibility of reforming within the SOFC, and this implies that SOFCs are tolerant to impurities (e.g., CO).

Recently, the use of non-fossil fuels, e.g., biofuel, biomass, and biogas, as energy sources for SOFCs has received much interest. For example, Papurello et al. [3] studied solid waste conversion to energy using biogas as a fuel. Furthermore, the use of biomass as a syngas source has been integrated with an SOFC system to produce electricity [4]. Biogas, which consists of 60% CH_4 and 40% CO_2, is one of the most attractive alternative fuels to use as a feedstock for stationary power (e.g., fuel cell applications) and combined heat and power (CHP) systems [5]. The presence of a large amount of CH_4 and a reforming agent (CO_2) in biogas means that it can be converted into a H_2-rich gas without a humidifier [6]. Biogas is renewable and a theoretically CO_2-neutral fuel derived from the anaerobic digestion of various kinds of organic waste, such as

---

* Corresponding author.
   E-mail address: yaneeporn.pa@kmitl.ac.th (Y. Patcharavorachot).

agricultural residues, food waste, animal waste, and municipal wastewater [7,8].

In general, biogas is first reformed to generate the H_2-rich gas that is required for the electrochemical reaction at the anode side of an SOFC. SOFCs are operated between 1023 and 1173 K, which is the temperature range used in reforming reactions. Therefore, biogas can be directly fed and reformed at the anode side of the cell. This approach is called direct internal reforming (DIR). There are two important features of this process: (1) The fuel is directly converted to electrical energy, resulting in the improvement of overall system efficiency, and (2) heat released from the electrochemical reaction can be supplied to the reforming reaction, thereby eliminating the need for an external heat source and cell cooling unit [9]. Because of the attractive operation of DIR SOFCs, a number of research groups have focused on their use with biogas as a fuel in recent years [10]. The DIRs of biogas in anode-supported SOFCs have been shown to provide good performance and a good conversion of CH_4 [11]. Shiratori et al. [6] presented an experimental study concerning the direct feeding of biogas to anode-supported button-cell SOFCs in which the dry reforming reaction was performed on the anode side. Their results revealed that, at a cell temperature of 800 °C and a current density of 200 mA/cm^2, the cell voltage fluctuated. This is because carbon formation on the anode material caused an increase in anodic overpotential. To overcome this problem, they proposed that adding air to biogas could reduce carbon formation. They also found that the cell voltage became more stable. Lanzini and Leone [12] confirmed the formation of carbon on the anode material for a planar SOFC using biogas directly as a fuel with no co-feeding of a reforming agent. They reported that a mixture stream consisting of 60% CH_4 and 40% CO_2 causes carbon formation over the full range of SOFC operating temperatures. Moreover, feeding a reforming agent (air, steam, or CO_2) with the biogas in order to avoid carbon formation on the anode material was explored. The results revealed that adding air at the anode could prevent carbon deposition. From a literature survey, it is clear that the main problem for internal reforming SOFCs is carbon formation on the anode material, which results in deactivation of the catalyst and deterioration of SOFC performance. Another problem is the large temperature difference within SOFC stacks, which is due to an imbalance between the endothermic and exothermic reactions, and may cause mechanical failure of the SOFC stack [13].

To mitigate the problems facing internal reforming SOFCs, biogas can be converted into H_2 using an external reformer before feeding into the SOFC at the anode side. This approach is referred to as external reforming. Although this process has lower system efficiency than that of internal reforming since the endothermic reforming and exothermic electrochemical reactions are carried out separately in different units, it presents some attractive features that should be considered. In an external reforming SOFC, not only electricity but also high temperature exhaust gases can be generated. The hot stream exiting from the SOFC can be further used as a heat source for cogeneration applications and bottoming cycles or integrated with a gas turbine, resulting in an improvement in the electrical and thermal efficiencies of system [14]. Furthermore, external reforming SOFCs present opportunities and challenges in terms of heat integration and control design. For example, Saebea et al. [15] analysed the performance of an external reforming SOFC in which an external biogas reformer was integrated. Furthermore, a thermodynamic study of biogas-fed SOFC systems using steam, air, and combined air/steam as reforming agents was performed to determine the most appropriate fuel processor [16]. The results showed that the most suitable reforming agent is steam, and that the power densities of steam-fed SOFCs are higher than air-fed SOFCs, even though their electrical efficiencies are slightly lower. The use of a biogas split

alternative to improve the electrical efficiency of SOFCs using steam as the reforming agent was explored. The results showed that a higher electrical efficiency could be achieved even if the power density is reduced. Farhad et al. [17] studied and compared electrical efficiencies of different SOFC micro-CHP systems. There are three methods considered in this system, i.e., anode exit gas recirculation, steam reforming, and partial oxidation. From simulation results, it was found that a micro-CHP SOFC system with anode exit gas recirculation provides the highest electrical efficiency, followed by that with steam reforming and then that with partial oxidation.

Since internal and external reforming SOFCs present different advantages and disadvantages, the purpose of this study was to investigate the electrical characteristics of biogas-fuelled SOFCs using the two different reforming approaches. Although the performances of external and internal reforming SOFCs have been investigated in many studies, a comparative study of different reforming approaches for biogas-fuelled SOFCs has not been reported. In this study, the optimal operating conditions for each approach are identified. Furthermore, in order to identify the most suitable reforming approach from an environmental perspective, the CO_2 and CO emissions for each approach are also considered.

2. Process description

Fig. 1 shows an integrated external biogas reformer and SOFC system that was designed in AspenPlus™. Biogas (FEED), which consists of 60% CH_4 and 40% CO_2, and water (WATER) are separately supplied to the heater (HEATER) and compressor (COMP) to reach the required temperature and pressure. Then, each stream exits from the compressor and is fed into the reformer where the steam reforming (SR) and water-gas shift (WGS) reactions lead to the generation of synthesis gas (SYNGAS), containing H_2, CH_4, CO, CO_2, and H_2O. In this study, the reformer is replicated by the *RGibbs* model, which can be used to calculate the equilibrium gas composition based on the minimizing Gibbs free energy method.

After the reforming reaction is complete, the synthesis gas (SYNGAS) is supplied to the SOFC at the anode side (ANODE) where the residual CH_4 can be further converted into H_2 via the SR reaction and the remaining CO produces more H_2 via the WGS reaction. Then, the oxidation of H_2 obtained from the SR and WGS reactions is performed. The anode is modelled by the *RGibbs* reactor, since there are three reactions occurring. Meanwhile, the syngas is fed to the anode side. Air (AIR) that is heated in the heater (HEATER4) and compressed in the compressor (COM3) is sent to the SOFC at the cathode side (CATHODE). In this work, the O_2 in air is required for the reduction reaction, and thus the *Sep* model is used to replicate the cathode. When O_2 from the cathode side (INANODE) is supplied to the anode, the overall electrochemical reaction is performed to produce electricity. It should be noted that, in the real operation of SOFCs, oxidation and reduction reactions occur at the anode and cathode, respectively, and are half-cell reactions. However, these reactions cannot be modelled in Aspen Plus simulations. Therefore, replacing the half-cell reactions with an overall electrochemical reaction is required [18].

A flowsheet for the biogas-fuelled internal reforming SOFC is shown in Fig. 2. Unlike the external reforming SOFC, biogas (FEED) and water (WATER) streams that are heated (HEATER) and compressed (COMP) can be directly supplied to the anode side of the SOFC (ANODE), whereas the heated and compressed air (AIR) is fed into the cathode side (CATHODE). O_2 in the air stream is isolated and sent to the anode side. Then, biogas at the anode side reacts with the steam and H_2 and CO are generated. In addition, CO reacts with the residual steam to produce more H_2 and CO_2. Finally, the H_2 produced reacts with O_2 to generate power. Table 1 shows the three
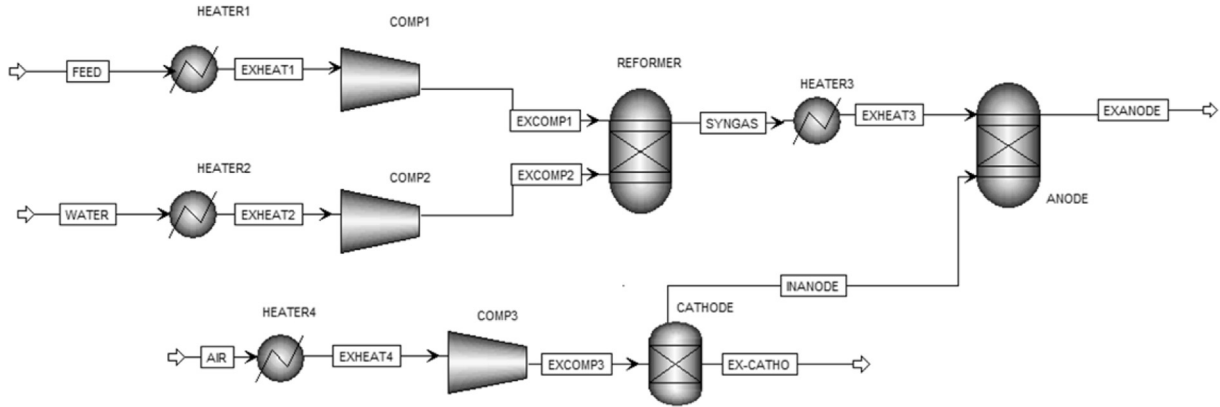
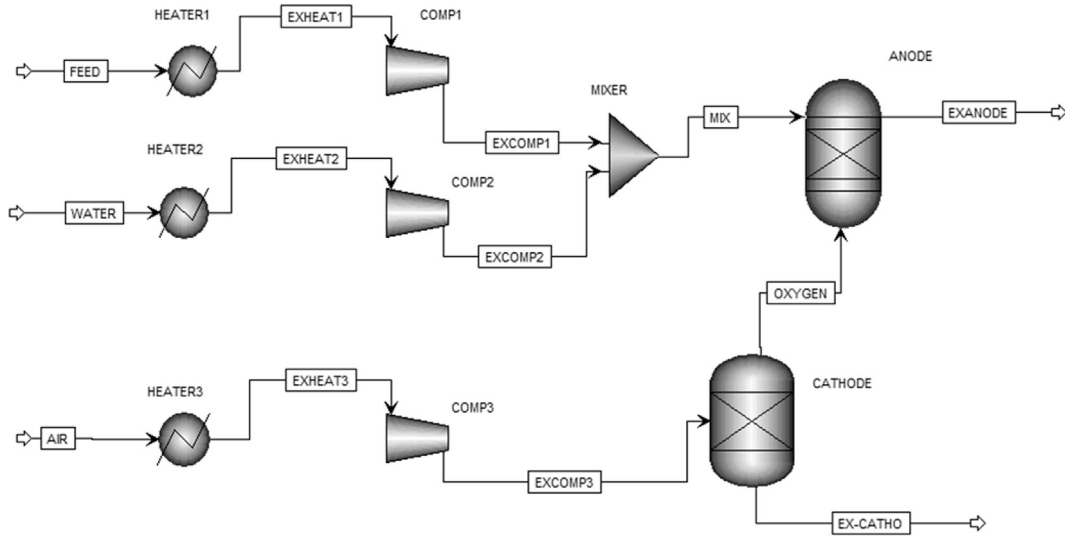**Fig. 1.** Flowsheet for the integrated external biogas reformer and SOFC system.

Fig. 2. Flowsheet for the biogas-fuelled internal reforming SOFC.

Table 1
Reactions occurring during SOFC operation.

Steam reforming	
$CH_4 + H_2O \leftrightarrow CO + 3H_2$	(1)
Water-gas shift	
$CO + H_2O \leftrightarrow CO_2 + H_2$	(2)
Overall electrochemical	
$H_2 + 0.5O_2 \leftrightarrow H_2O$	(3)

chemical reactions occurring in the SOFC, including the SR, WGS, and overall electrochemical reactions.

3. Electrochemical model of the SOFC

In this study, an electrochemical model, which shows the relationship of the fuel conversions to electrical energy, is used to analyse the performance of each process. The following assumptions have been defined to represent the SOFC model: zero-dimensional model; steady state operation; negligible pressure drops; SR and WGS reactions considered at equilibrium; and only oxidation of H_2.

The electrical performance of an SOFC can be characterized by its actual cell voltage (V), which can be determined when the current density is given. The actual cell voltage of an SOFC is always less than the theoretical potential or open-circuit voltage (E^{OCV}) because of the three main losses encountered in SOFC operation: anode and cathode activation overpotentials, ohmic loss, and anode and cathode concentration overpotentials. The E^{OCV}, being the maximum voltage, can be determined by the Nernst equation:

$$E^{OCV} = E^0 + \frac{RT}{2F}\ln\left(\frac{p_{H_2}p_{O_2}^{1/2}}{p_{H_2O}}\right) \quad (4)$$

where R is the gas constant, F is the faraday constant (9.6485×10^4 C/mol), T is the cell temperature, p_i is the partial pressure of component i, and E^0 is the reversible open-circuit voltage at standard temperature and pressure, which can be expressed by Eq. (5) [19]:

$$E^0 = 1.253 - 2.4516 \times 10^{-4}T \quad (5)$$

Considering the three losses in the SOFC operation, the actual

cell operating voltage can be calculated by

$$V = E^{OCV} - (\eta_{activation} + \eta_{ohmic} + \eta_{concentration}) \tag{6}$$

where $\eta_{activation}$, η_{ohmic}, and $\eta_{concentration}$ are the activation, ohmic, and concentration overpotentials.

Activation loss ($\eta_{activation}$) is caused by the electrochemical reactions at the electrodes. It can be calculated using the nonlinear Butler-Volmer equation:

$$i = i_{0,electrode} \left[\exp\left(\frac{\alpha nF}{RT} \eta_{activation,electrode} \right) - \exp\left(-\frac{(1-\alpha)nF}{RT} \eta_{activation,electrode} \right) \right] \tag{7}$$

where i is the current density. The exchange current density at the electrodes ($i_{0,electrode}$), proposed by Aguiar et al. [9], can be calculated as a function of cell temperature, pre-exponential factor ($k_{electrode}$), and activation energy ($E_{electrode}$), as follows:

$$i_{0,electrode} = \frac{RT}{nF} k_{electrode} \exp\left(-\frac{E_{electrode}}{RT} \right) \tag{8}$$

$$electrode \in \{anode, cathode\}$$

The values of the pre-exponential factor and activation energy for the calculation of $i_{0,electrode}$ are listed in Table 2.

The voltage loss caused by the resistance to the oxygen ions diffusing through the electrolyte and the electrons flowing through the cell components is termed ohmic loss (η_{ohmic}). This loss can be calculated from the current density and the internal resistance of the cell (R_{ohm}). R_{ohm} is calculated from the effective distance between the components coupled with conductivity data. Thus, the ohmic loss is given by

$$\eta_{ohmic} = iR_{ohm}$$
$$R_{ohm} = \frac{\tau_{anode}}{\sigma_{anode}} + \frac{\tau_{electrolyte}}{\sigma_{electrolyte}} + \frac{\tau_{cathode}}{\sigma_{cathode}} \tag{9}$$

where τ_i is the thickness of cell component i (i.e., anode, electrolyte, or cathode) and σ represents the electronic conductivity (σ_{anode} and $\sigma_{cathode}$) and ionic conductivity ($\sigma_{electrolyte}$).

Concentration loss ($\eta_{concentration}$) occurs due to the faster consumption of the reactants at the electrode/electrolyte interface. It can be estimated from the difference in conditions as compared to the open-circuit potential calculation. The different conditions for the Nernst equation are the concentrations of reactant and product at the three-phase boundary (TPB) and the bulk concentration. This loss can be calculated using Eq. (10):

$$\eta_{concentration} = \frac{RT}{2F} \ln\left(\frac{p_{H_2O,TPB}p_{H_2}}{p_{H_2O}p_{H_2,TPB}} \right) + \frac{RT}{4F} \ln\left(\frac{p_{O_2}}{p_{O_2,TPB}} \right) \tag{10}$$

where the terms of the right-hand side represent the anode and the

Table 2
Pre-exponential factors and activation energies used for calculating exchange current densities [9].

$k_{cathode}$	2.35×10^{11} 1/Ω m^2	$E_{cathode}$	137 kJ/mol
k_{anode}	6.54×10^{11} 1/Ω m^2	E_{anode}	140 kJ/mol

cathode concentration overpotentials, respectively. The relationships between the partial pressures of H_2, H_2O, and O_2 at the TPB and the current density are shown in Eqs. (11)–(13).

$$p_{H_2,TPB} = p_{H_2} - \frac{RT\tau_{anode}}{2F\overline{D}_{eff,anode}} i \tag{11}$$

$$p_{H_2O,TPB} = p_{H_2O} + \frac{RT\tau_{anode}}{2F\overline{D}_{eff,anode}} i \tag{12}$$

$$p_{O_2,TPB} = P - (P - p_{O_2}) \exp\left(\frac{RT\tau_{cathode}}{4FD_{eff,cathode}P} i \right) \tag{13}$$

where $\overline{D}_{eff,anode}$ is the average effective gas diffusivity coefficient in the anode (a binary gas mixture of H_2 and H_2O) and $D_{eff,cathode}$ is the effective gas diffusivity coefficient in the cathode (a gas mixture of O_2 and N_2). The effective diffusivity coefficient in the electrode ($D_{eff,electrode}$) is related to the molecular diffusivity ($D_{molecular}$), as given by

$$D_{eff,electrode} = \frac{\varepsilon_p}{\tau_{tortuosity}} D_{molecular,i}, \; i \in \{H_2, H_2O, O_2, N_2\} \tag{14}$$

In addition, the molecular diffusivity is also related to the bulk diffusivity (D_{bulk}) and Knudsen diffusivity ($D_{knudsen}$) by

$$\frac{1}{D_{molecular,i}} = \frac{1}{D_{bulk,i}} + \frac{1}{D_{knudsen,i}}, \; i \in \{H_2, H_2O, O_2, N_2\} \tag{15}$$

4. Methodology

In this study, the flowsheet for each system was designed using Aspen Plus simulation software based on thermodynamic calculations. In the case of the external reforming SOFC, the computation is divided into two steps. First, the reformer conditions, i.e., steam-to-carbon (S/C) molar ratio, temperature, and pressure, determine the gas composition in the reforming process at equilibrium based on the Gibbs free energy minimization method. Furthermore, the CH_4 (x_{CH4}), CO (x_{CO}), and H_2 (x_{H2}) compositions obtained from the reformer are employed for the SOFC calculation, since these components are associated with H_2 generation at the anode side. To calculate the performance of SOFC, the electrochemical equations given in Section 3 are written in a calculator block installed in AspenPlus™. Finally, the SOFC performance in terms of cell voltage (V), power density (P_{SOFC}), and SOFC electrical efficiency (ε_{SOFC}) can be determined, as the operating conditions of the SOFC (i.e., cell temperature, pressure, and current density) and the physical parameters of the cell components (i.e., thicknesses and cell conductivities) are given. The performance factors, which include power density and SOFC electrical efficiency, are expressed as follows:

$$P_{SOFC} = iV \tag{16}$$

$$\varepsilon_{EX-SOFC} = \frac{P_{SOFC}A}{(x_{CH_4}LHV_{CH_4} + x_{H_2}LHV_{H_2} + x_{CO}LHV_{CO})F_{fuel}} \times 100\% \tag{17}$$

where $\varepsilon_{EX-SOFC}$ represents the electrical efficiency of the external reforming SOFC, A is the active area of the SOFC, F_{fuel} is the inlet molar flow rate of the fuel stream at the fuel cell, and LHV_i stands for the lower heating value of component i.

For the internal reforming SOFC, biogas can be reformed to H_2 and directly converted into electrical energy, and thus only the SOFC calculation is considered. Like the calculation of SOFC performance in the external reforming SOFC, the cell voltage, power density, and SOFC electrical efficiency can be calculated. The electrical efficiency of an internal reforming SOFC can be calculated and expressed as:

$$\varepsilon_{IN-SOFC} = \frac{P_{SOFC}A}{x_{CH_4}LHV_{CH_4}F_{fuel}} \times 100\% \tag{18}$$

where $\varepsilon_{IN-SOFC}$ represents the electrical efficiency of the internal reforming SOFC. It is noted that the composition of the anode exhaust gas obtained from both processes can be calculated based on the Gibbs free energy minimization method.

5. Model validation

In the case of the external reforming SOFC, the process is composed of two parts: the external biogas reformer and the SOFC. In order to ensure that the proposed model in the Aspen Plus simulation can predict the H_2 production from the external reformer and the power generation of the SOFC, a comparison of the results obtained from the proposed model and experimental data from the literature was performed.

Firstly, the model prediction was validated with the experimental data from Kolbitsch et al. [20], who studied H_2 production from biogas ($CH_4/CO_2 = 60/40$) using a temperature range of 923–1123 K, an S/C molar ratio of 2, and atmospheric pressure. They found that the H_2-rich synthesis gas contained H_2, CO, CO_2, and CH_4. Fig. 3 shows a comparison between the model prediction and the experimental results, demonstrating that the model prediction agrees well with the experimental data. The results indicate that the maximum deviation of the H_2 production calculated using the simulation from that in the experimental data is 12%.

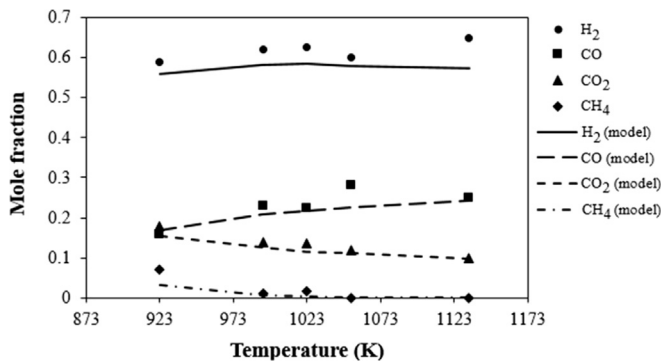For the SOFC model, the results obtained from the simulation were compared with the experimental data from Zhao and Virkar [21]. An inlet fuel consisting of 97% H_2 and 3% H_2O and an inlet oxidant consisting of 21% O_2 were fed in their study. The anode, electrolyte, and cathode had thicknesses of 1000, 8, and 20 μm, respectively. This configuration is termed an anode-supported SOFC. The result in terms of cell voltage from the proposed model compared with the experimental data as a function of current density at different operating temperatures is shown in Fig. 4. It can be seen that the simulated results and experimental data agree well over the entire temperature range studied. The maximum deviations of cell voltage from the experimental data are 15, 8, and 6% at operating temperatures of 873, 973, and 1073 K, respectively.

It is noted that, since there are deviations between the model predictions and the experimental data, the real efficiency of the SOFC system and the CO_2 and CO emissions would be lower than the predicted value.

6. Results and discussion

Table 3 illustrates the model parameter values used to analyse the performance of the external and internal reforming SOFCs at nominal conditions. Note that the values of cell geometry and structural parameters for the SOFCs are taken from our previous works [15,22]. This section is divided into three parts. Section 6.1 presents the performance analysis for the external reforming SOFC with respect to a wider range of operating conditions in the reformer and SOFC. The effect of SOFC operating conditions on the performance of the internal reforming SOFC is presented in Section 6.2. Finally, a comparative study of the different reforming approaches in terms of performance and environmental effect is presented in Section 6.3.

6.1. External reforming SOFC

For the performance analysis of the external reforming SOFC, the impact of the operating conditions for the reformer (i.e., temperature and S/C molar ratio) and SOFC (i.e., current density, temperature, and pressure) on H_2 production and power generation have been investigated. Fig. 5 presents the H_2 production, cell voltage, power density, and SOFC efficiency as a function of reformer temperature. The reformer temperature is varied from 873 to 1073 K while the other parameters presented in Table 3 are kept constant. As expected, more H_2 is produced when the reformer is operated at higher temperature, as demonstrated in Fig. 5a. The SR reaction is endothermic and thus favourable under higher temperature operation, so this reaction moves toward the product side. This leads to higher H_2 production. When more H_2 is
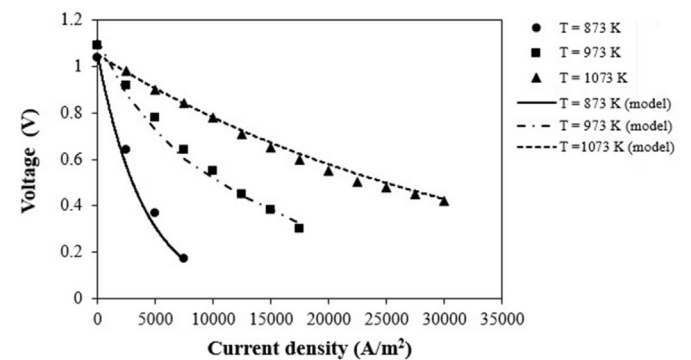

Fig. 3. Comparison between the model prediction and experimental result of Kolbitsch et al. [20] for H_2 production from biogas reforming.

Fig. 4. Comparison between the model prediction and experimental result of Zhao and Virkar [21] for power generation from an SOFC.

Table 3
Model parameter used in this study under standard conditions.

Parameters	Value	Unit
Operating conditions of Reformer		
Reformer temperature	973	K
Reformer pressure	1	atm
Steam to carbon molar ratio (S/C)	0.5	−
Operating conditions of SOFC		
SOFC temperature	1073	K
SOFC pressure	1	atm
Current density	5000	A/m^2
Cell dimensions of SOFC		
Active area	55.2	m^2
Anode thickness	500	μm
Cathode thickness	40	μm
Electrolyte thickness	40	μm
Material properties of SOFC		
Anode diffusion coefficient	3.66×10^{-5}	m^2/s
Cathode diffusion coefficient	1.37×10^{-5}	m^2/s
Anode electrical conductivity	$\frac{4.2 \times 10^7}{T} \exp\left(-\frac{1200}{T}\right)$	1/Ω m
Cathode electrical conductivity	$\frac{9.5 \times 10^7}{T} \exp\left(-\frac{1150}{T}\right)$	1/Ω m
Electrolyte ionic conductivity	$33.4 \times 10^3 \exp\left(-\frac{10300}{T}\right)$	1/Ω m

Fig. 5. Effect of reformer temperature in external reforming SOFC on: (a) H$_2$ production, (b) cell voltage and power density, and (c) SOFC efficiency.

supplied to the SOFC stack, the open-circuit voltage is higher. Furthermore, the concentration overpotential can be decreased as more H$_2$ can easily diffuse to the reaction site. This causes an increase in the cell voltage followed by an increase in power density, as seen in Fig. 5b. Conversely, Fig. 5c shows that the SOFC efficiency slightly decreases with an increase in the reformer temperature. The current density is fixed as constant in this study, while the total inlet molar flow rate of fuel (including the molar flow rates of CH$_4$, CO, and H$_2$) increases with an increase in the temperature of the reformer. This means that the extent of conversion of fuel to electrical energy decreases, which reduces the SOFC efficiency. In order to achieve a compromise between the power density and the electrical efficiency of the SOFC, a reformer temperature of 973 K is selected. This temperature is also used in the next study.

Fig. 6 shows the effect of S/C molar ratio on the H$_2$ production, cell voltage, power density, and efficiency of the SOFC. In this study, the S/C molar ratio is adjusted between 0.5 and 5 while the other parameters shown in Table 3 are set as a constant. From the simulation result shown in Fig. 6a, the mole fraction of H$_2$ improves when the S/C molar ratio is increased from 0.5 to 1, and then decreases thereafter. An increase in the S/C molar ratio can shift the equilibrium of the SR reaction to the product side and this leads to higher H$_2$ production. Furthermore, higher steam content will react with more CO to produce more H$_2$ and CO$_2$. Thus, Fig. 6a shows a decrease in CO and an increase in CO$_2$. However, the residual steam will dilute the H$_2$, i.e., the mole fraction of H$_2$ is lower when the S/C molar ratio is higher. Furthermore, the open-circuit voltage decreases due to an increase in the concentration overpotential when a fuel stream with less H$_2$ is provided to the SOFC. This leads to a reduction in cell voltage, power density, and SOFC efficiency, as seen in Fig. 6b and c. Therefore, an S/C molar ratio of 0.5 provides sufficient power density and SOFC efficiency.

Next, the effect of SOFC operating conditions on power generation is investigated. Fig. 7 illustrates the electrical characteristics of the SOFC under the nominal conditions ($T = 1073$ K and $P = 1$ atm) at different current densities. In this study, the synthesis gas obtained from the reformer operated at a temperature of 973 K, pressure of 1 atm, and S/C molar ratio of 0.5 is fed into the SOFC stack operated at a temperature of 1073 K and at atmospheric pressure. The simulation results reveal that an increase in the current density causes a decrease in the cell voltage. There are
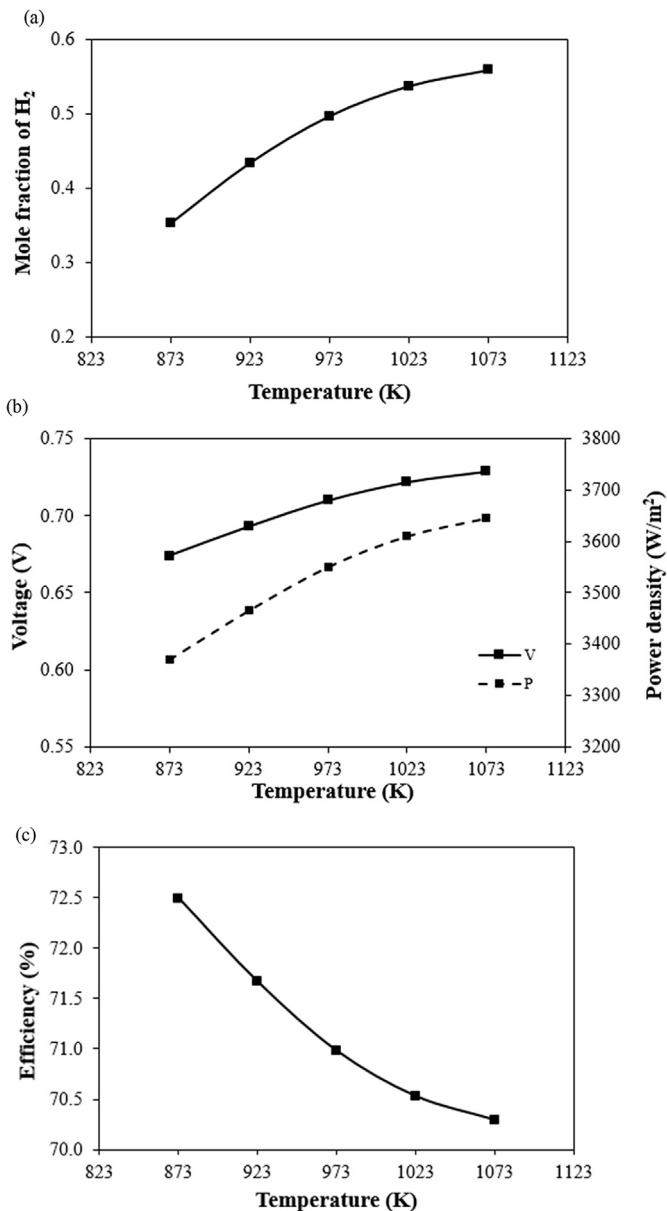
increases in the three voltage losses with increasing current density, since the activation overpotentials, ohmic loss, and concentration overpotentials are proportional to current density. The power density increases initially and reaches a maximum value of 5600 W/m^2 at a current density of 9000 A/m^2, after which it decreases with decreasing cell voltage. Although the SOFC operated at a current density of 9000 A/m^2 provides the maximum power density, SOFCs are commonly operated at 0.7 V to provide a suitable compromise between power density, cell efficiency, capital cost, and stable operation [9]. Therefore, a current density of 5000 A/m^2 is selected since a cell voltage of 0.7 V can be achieved.

The influence of SOFC temperature and pressure on the cell voltage, power density, and SOFC efficiency is presented in Fig. 8. It can be seen that an increase in SOFC temperature in the range 1073−1273 K under atmospheric pressure improves the performance of the SOFC. This is mainly caused by an increase in the open-circuit voltage and a decrease in the activation and ohmic
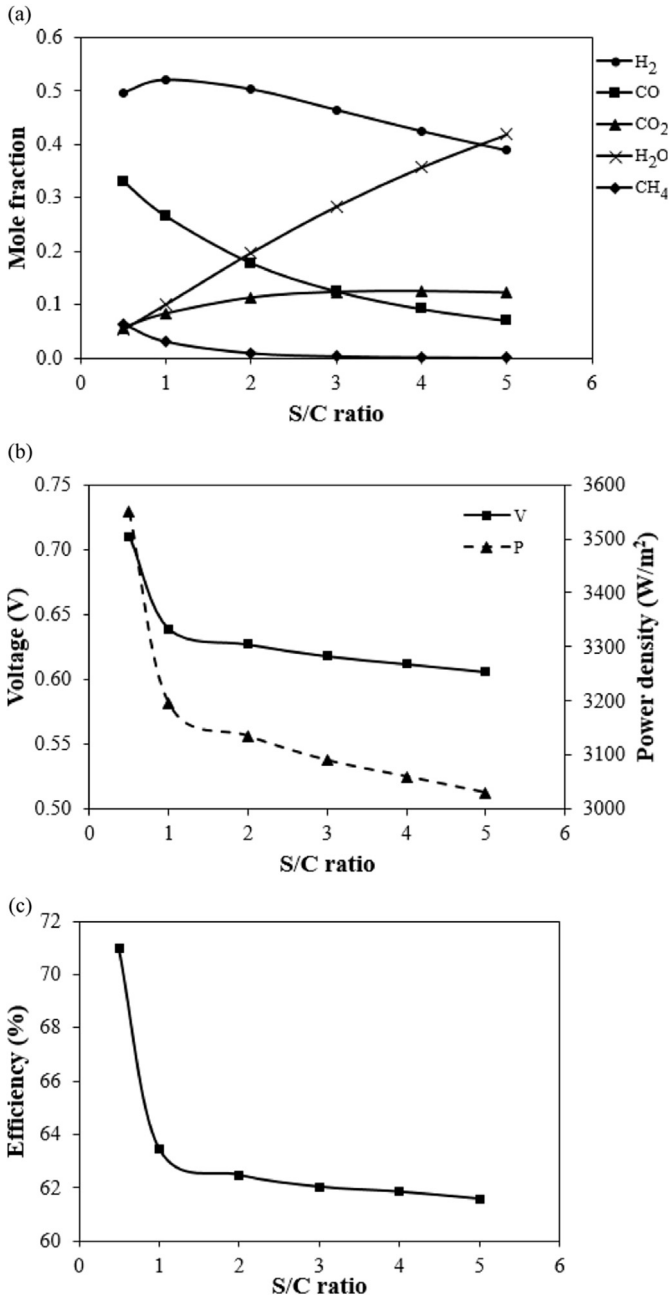
(a)

(b)

(c)

Fig. 6. Effect of steam-to-carbon molar ratio in an external reforming SOFC on: (a) H_2 production, (b) cell voltage and power density, and (c) SOFC efficiency.
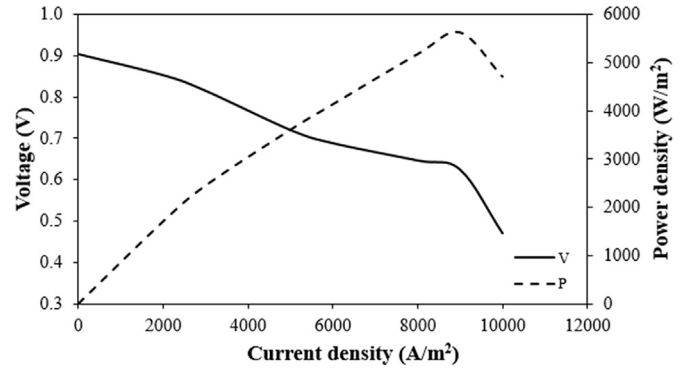

Fig. 7. Performance characteristics of an external reforming SOFC with different current densities at an SOFC temperature of 1073 K and an SOFC pressure of 1 atm.
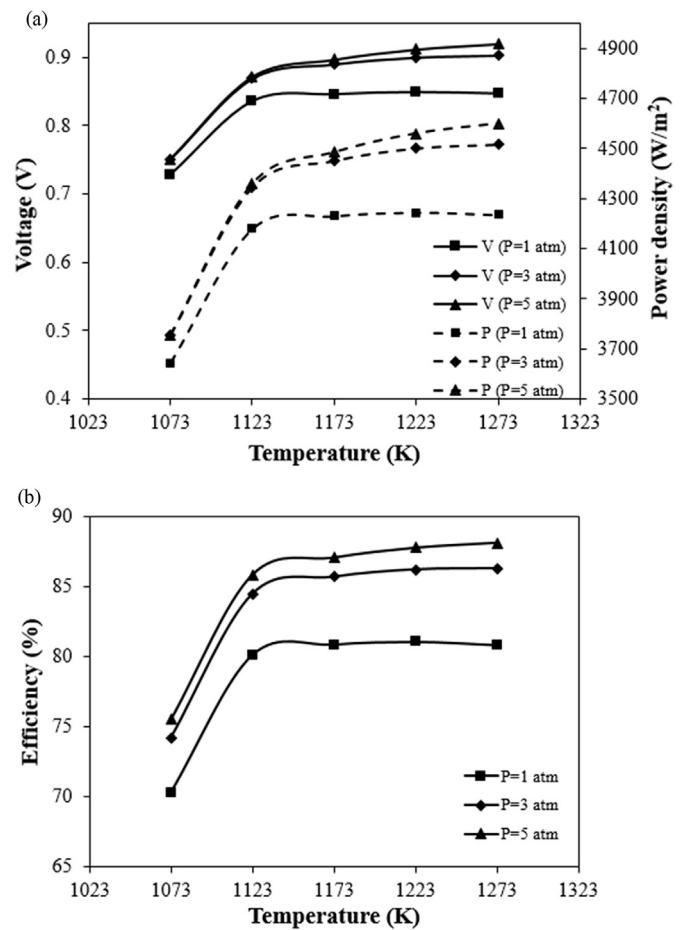
(a)

(b)

Fig. 8. Effect of temperature and pressure of an external reforming SOFC on: (a) cell voltage and power density and (b) SOFC efficiency.

overpotentials. Operating an SOFC at higher temperatures can decrease the activation overpotential due to an increase in the reaction rate as well as a decrease the ohmic overpotential since the conductivity of the electrodes and electrolyte is increased. However, the concentration overpotential increases with an increase in the SOFC temperature, since the gas-diffusion coefficient used in Eqs. (11)–(13) is independent of the operating temperature. An increase in the concentration overpotential has less effect compared with that of the others, and thus the SOFC performance is enhanced. Moreover, Fig. 8 also shows SOFC performance of as a function of SOFC pressure, which is varied from 1 to 5 atm. The simulation results indicate that cell voltage, power density, and cell efficiency can be enhanced when the SOFC is operated at higher pressure. The increasing pressure in the SOFC will increase the

open-circuit voltage of the SOFC, while the concentration overpotential can be reduced since the gas diffusion from the bulk to the interface is easier. This leads to an increase in the cell voltage, thus increasing the power density and cell efficiency. The simulation results show that the most favourable operating conditions for the SOFC are elevated temperature and pressure. However, the SOFC should be operated at $T = 1173$ K and $P = 3$ atm to compromise between SOFC performance, cost, and cell durability. Under these operating conditions, power density of 4450 W/m^2 and cell efficiency of ~86% are obtained.

6.2. Internal reforming SOFC

The impact of the temperature and pressure of the SOFC and the S/C molar ratio on cell performance is determined. Fig. 9 shows the H₂ production and SOFC performance of the internal reforming SOFC at different S/C ratios. The S/C molar ratio is changed from 0.5 to 5 while the other parameters in Table 3 are kept at a constant value. As seen in Fig. 9a, increasing the S/C molar ratio results in a significant decrease in H₂ production. This is because the H₂ is diluted when the SOFC is fed with higher steam content. The mole fraction of CO shows a similar trend to that for H₂, whereas more CO₂ is produced when the S/C molar ratio is higher. Because H₂ concentration decreases with increasing S/C molar ratio, the cell voltage and power density decrease, as expressed in Fig. 9b. In this operation, the molar flow rate of CH₄ at the inlet of the SOFC is set at a constant value, and thus the reduction of power density leads to a decrease in the electrical efficiency of the SOFC, as dictated by Eq. (18). The results show that an S/C molar ratio of 0.5 provides good

SOFC performance.

Next, the influences of SOFC temperature and pressure on performance of the internal reforming SOFC are examined, as demonstrated in Fig. 10. The values of SOFC temperature and pressure are changed while the other parameters shown in Table 3 are kept constant. For the internal reforming SOFC, when a mixture of biogas and steam is fed into the SOFC stack, the SR and WGS reactions occur at the anode side. Therefore, H₂ and CO are produced. After the biogas is completely consumed, the electrochemical reaction is more pronounced and this leads to the consumption of H₂ to generate electrical energy. The simulation results indicate that increasing the SOFC temperature from 1073 to 1273 K under atmospheric pressure causes increases in the cell voltage, power density, and electrical efficiency of the SOFC. This can be explained by the improved open-circuit potential and the reduction of activation and ohmic losses with increasing SOFC temperature. However, the performance of the SOFC drops dramatically when it is operated at 1273 K. Higher concentration overpotential is observed under these conditions, and thus the cell voltage is decreased and this causes a decrease in the power density and cell efficiency. Furthermore, the performance of the SOFC operated at 1173 K is close to that at 1223 K, and thus a temperature of 1173 K is a good operating point. Fig. 10 also shows the effect of changing SOFC pressure (in the range 1–5 atm) on SOFC performance. Under a constant SOFC temperature, higher-pressure operation improves the SOFC performance in terms of the cell voltage, power density, and electrical efficiency. This is due to an increase in the open-circuit voltage and a decrease in the concentration overpotential. However, the performance of the SOFC operated at 3 atm is close to that at 5 atm; therefore, an operating pressure of 3 atm should be selected to prevent the failure of the SOFC stack and to reduce fixed and operating costs. Under the optimal SOFC operating conditions of 1173 K and 3 atm, the internal
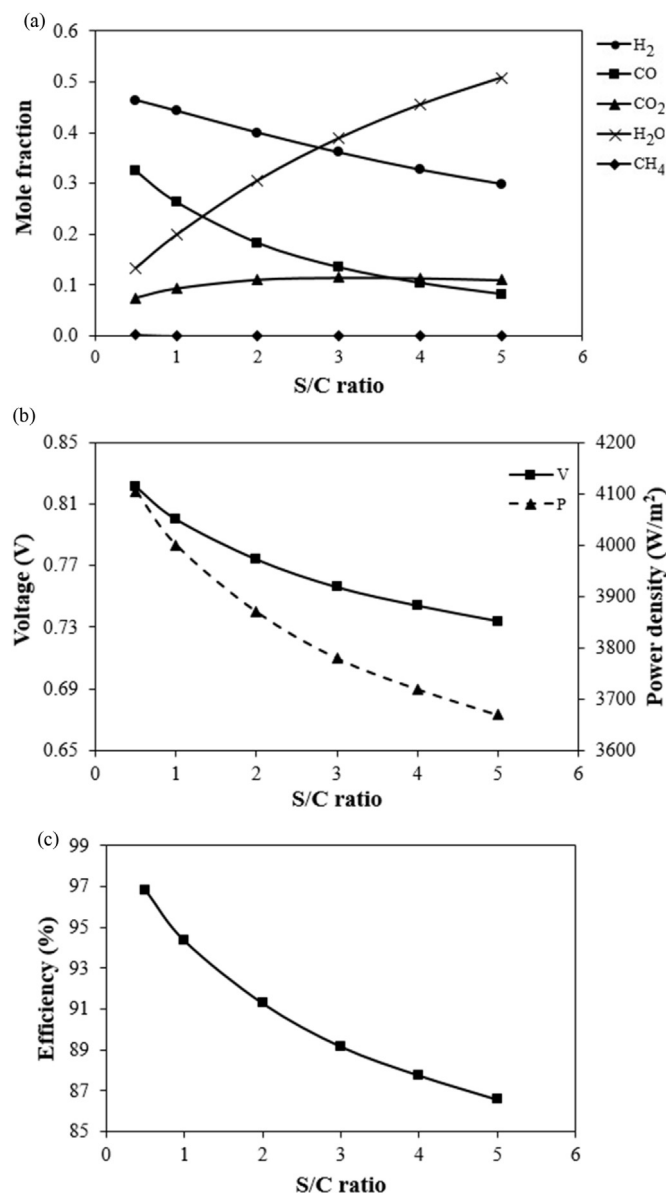

Fig. 9. Effect of steam to carbon molar ratio in an internal reforming SOFC on: (a) H₂ production, (b) cell voltage and power density, and (c) SOFC efficiency.
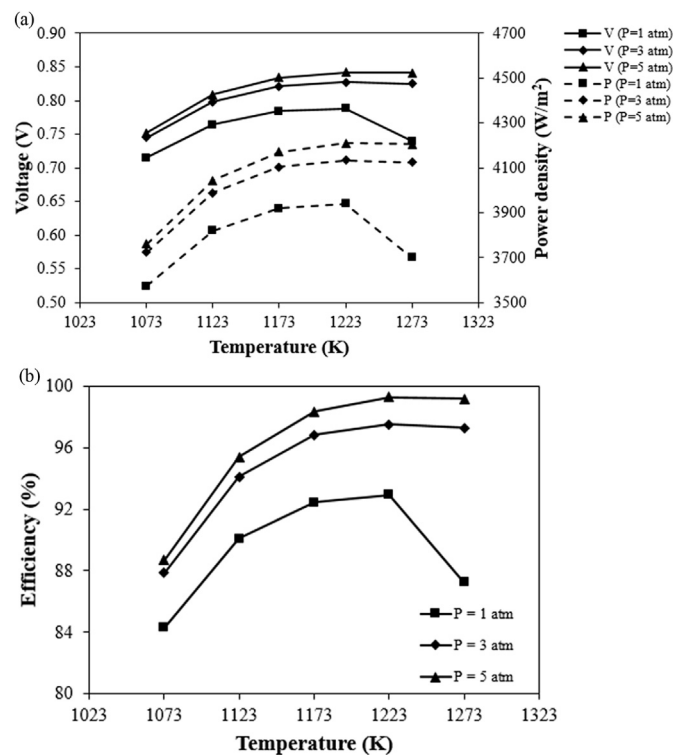

Fig. 10. Effect of temperature and pressure of an internal reforming SOFC on: (a) cell voltage and power density, and (b) SOFC efficiency.

reforming SOFC can provide a power density and cell efficiency of 4105 W/m^2 and 97%, respectively.

6.3. Comparison of performance and environmental effect of the different approaches

For the external reforming SOFC, the reformer should be operated at a temperature of 973 K, atmospheric pressure, and an S/C molar ratio of 0.5, and the optimal operating conditions for the SOFC are a temperature, pressure, and current density of 1173 K, 3 atm, and 5000 A/m^2, respectively. Under these operating conditions, the external reforming SOFC can provide a power density and cell efficiency of 4450 W/m^2 and ~86%, respectively. For the internal reforming SOFC, the SOFC should be operated at temperature of 1173 K, a pressure of 3 atm, and current density of 5000 A/m^2 with an S/C molar ratio of 0.5, providing a power density of 4105 W/m^2 and a cell efficiency of 97%. Comparing the performances of the external and internal reforming SOFCs indicates that the internal reforming SOFC has a higher electrical efficiency. The internal reforming SOFC performs a one-step conversion of fuel to electricity. Therefore, improved cell efficiency is observed. In addition, the elimination of the reformer unit is a significant feature of this operation. However, when the power densities are compared, it is clear that the external reforming SOFC has a higher power density. This implies that the external reforming SOFC requires a smaller active area.

Next, the environmental effects of each reforming operation in terms of CO_2 and CO emissions from the exhaust gas at the anode side are compared, as shown in Fig. 11. Under the same operating condition, the SOFC operated with internal reforming releases 7.4% CO_2 and 37.9% CO, whereas 1.9% CO_2 and 32.5% CO are released with external reforming. Thus, it is concluded that the internal reforming SOFC releases more CO_2 and CO than the external reforming SOFC. However, it should be noted that in these simulations, the consumption of H_2 to produce electricity was fixed by setting a constant current density. Although more H_2 is produced in the internal reforming SOFC, it is used in the same quantity. Thus, there is more undepleted H_2 present in the anode exhaust gas. This may lead to higher amounts of CO_2 and CO.

7. Conclusions

This study presented the performance and environmental
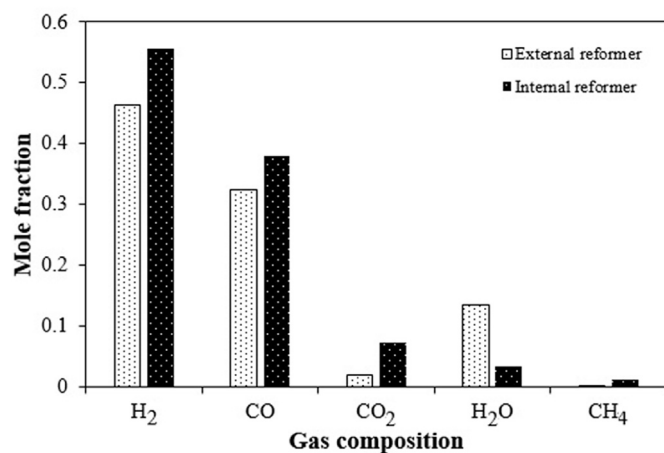

Fig. 11. Comparison of gas compositions in the anode exhaust gas obtained from different reforming approaches when the SOFC is operated at a temperature of 1173 K, a pressure of 3 atm, and a current density of 5000 A/m^2.

analysis of biogas-fuelled SOFC systems incorporating different reforming approaches, i.e., external and internal reforming. The Aspen Plus simulator was used to determine the optimal operating conditions based on thermodynamic calculations for each process. The calculator block was also used to model the electrochemical reaction in the SOFC. The impacts of operating conditions for the external and internal reforming SOFCs on H_2 production and power generation were determined. Further, the emission of CO_2 and CO was investigated. The simulation results for the external reforming SOFC indicated that the reformer should be operated at 973 K with an S/C molar ratio of 0.5 while the optimal operating conditions for the SOFC were determined to be 1173 K and 3 atm with current density of 5000 A/m^2. These conditions represent a good compromise between power density and electrical efficiency. Moreover, the optimal operating conditions for the internal reforming SOFC are the same as those for the external reforming SOFC. Under the same operating conditions, the electrical efficiency of the internal reforming SOFC (97%) is superior to that of the external reforming SOFC (86%). Finally, the internal reforming SOFC releases more CO_2 and CO than the external reforming SOFC.

These results clearly show that both reforming approaches have different strengths, and that the electrical performance and environmental effects should be compromised to obtain a highly efficient and clean technology.

Acknowledgments

References

[1] Hauptmeier K, Penkuhn M, Tsatsaronis G. Economic assessment of a solid oxide fuel cell system for biogas utilization in sewage plants. Energy 2016;117:361—8.

[2] Baldinelli A, Barelli L, Bidini G. Performance characterization and modelling of syngas-fed SOFCs (solid oxide fuel cells) varying fuel composition. Energy 2015;90:2070—84.

[3] Papurello D, Lanzini A, Tognana L, Silvestri S, Santarelli M. Waste to energy: exploitation of biogas from organic waste in a 500 W$_{el}$ solid oxide fuel cell (SOFC) stack. Energy 2015;85:145—58.

[4] Din ZU, Zainal ZA. Biomass integrated gasification—SOFC systems: technology overview. Renew Sust Energy Rev 2016;53:1356—76.

[5] Papadias DD, Ahmed S, Kumar R. Fuel quality issues with biogas energy — an economic analysis for a stationary fuel cell system. Energy 2012;14:257—77.

[6] Shiratori Y, Ijichi T, Oshima T, Sasaki K. Internal reforming SOFC running on biogas. Int J Hydrogen Energy 2010;35:7905—12.

[7] Saebea D, Authayanun S, Patcharavorachot Y, Arpornwichanop A. Enhancement of hydrogen production for steam reforming of biogas in fluidized bed membrane reactor. Chem Eng Trans 2014;39:1177—82.

[8] Santos IFS, Barros RM, Filho GLT. Electricity generation from biogas of anaerobic wastewater treatment plants in Brazil: an assessment of feasibility and potential. J Clean Prod 2016;126:504—14.

[9] Aguiar P, Adjiman CS, Brandon NP. Anode-supported intermediate temperature direct internal reforming solid oxide fuel cell. I: model-based steady-state performance. J Power Sources 2004;138:120—36.

[10] Shiratori Y, Ogura T, Nakajima H, Sakamoto M, Takahashi Y, Wakita Y, et al. Study on paper-structured catalyst for direct internal reforming SOFC fueled by the mixture of CH_4 and CO_2. Int J Hydrogen Energy 2013;38:10542—51.

[11] Santarelli M, Quesito F, Novaresio V, Guerra C, Lanzini A, Beretta D. Direct reforming of biogas on Ni-based SOFC anodes: modelling of heterogeneous reactions and validation with experiments. J Power Sources 2013;242: 405—14.

[12] Lanzini A, Leone P. Experimental investigation of direct internal reforming of biogas in solid oxide fuel cells. Int J Hydrogen Energy 2010;35:2463—76.

[13] Chatrattanawet N, Skogestad S, Arpornwichanop A. Control structure design and controllability analysis for solid oxide fuel cell. Chem Eng Trans 2014;39: 1291—6.

[14] Saebea D, Authayanun S, Patcharavorachot Y, Arpornwichanop A. Effect of anode-cathode exhaust gas recirculation on energy recuperation in a solid

oxide fuel cell-gas turbine hybrid power system. Energy 2016;94:218—32.

[15] Saebea D, Authayanun S, Patcharavorachot Y, Paengjuntuek W, Arpornwichanop A. Use of different renewable fuels in a steam reformer integrated into a solid oxide fuel cell: theoretical analysis and performance comparison. Energy 2013;51:305—13.

[16] Piroonlerkgul P, Assabumrungrat S, Laosiripojana N, Adesina AA. Selection of appropriate fuel processor for biogas-fuelled SOFC system. Chem Eng J 2008;140:341—51.

[17] Farhad S, Hamdullahpur F, Yoo Y. Performance evaluation of different configurations of biogas-fuelled SOFC micro-CHP systems for residential applications. Int J Hydrogen Energy 2010;35:3758—68.

[18] Doherty W, Reynolds A, Kennedy D. Computer simulation of a biomass gasification-solid oxide fuel cell power system using Aspen Plus. Energy 2010;35:4545—55.

[19] Ni M, Leung MKH, Leung DYC. Parametric study of solid oxide fuel cell performance. Energy Convers Manage 2007;48:1525—35.

[20] Kolbitsch P, Pfeifer C, Hofbauer H. Catalytic steam reforming of model biogas. Fuel 2008;87:701—6.

[21] Zhao F, Virkar AF. Dependence of polarization in anode supported solid oxide fuel cells on various cell parameters. J Power Sources 2005;141:79—95.

[22] Patcharavorachot Y, Arpornwichanop A, Chuachuensuk A. Electrochemical study of a planar solid oxide fuel cell: role of support structures. J Power Sources 2008;177:254—61.

Nomenclature

A: Active area of cell (m^2)
$D_{eff,electrode}$: Effective diffusion coefficient in electrode (m^2/s)
$D_{bulk,i}$: Bulk diffusivity coefficient of species i (m^2/s)
$D_{knudsen,i}$: Knudsen diffusion coefficient of species i (m^2/s)
$D_{molecular,i}$: Molecular diffusivity coefficient of species i (m^2/s)
E^0: Open-circuit potential at the standard pressure (V)
E^{OCV}: Open-circuit voltage (V)
E_{anode}: Activation energy for the anode (kJ/mol)
$E_{cathode}$: Activation energy for the cathode (kJ/mol)
F: Faraday's constant (9.6485 $\times$ 10^4 C/mol)
F_{fuel}: Molar flow rate of the fuel stream (kmol/h)
i: Current density (A/m^2)
$i_{0,anode}$: Exchange current density at the anode (A/m^2)
$i_{0,cathode}$: Exchange current density at the cathode (A/m^2)
k_{anode}: Pre-exponential factor at the anode (1/Ω m^2)
$k_{cathode}$: Pre-exponential factor at the cathode (1/Ω m^2)
LHV_i: Lower heating value of component i (kJ/mol)
n: number of electrons transferred
P: Operating pressure (atm)
p_i: Partial pressure of species i (atm)
$p_{i,TPB}$: Partial pressure at three phase boundaries of species i (atm)
P_{SOFC}: power density (W/m^2)
R: Universal gas constant
R_{ohm}: Internal resistance of the cell (Ω m^2)
T: Cell operating temperature (K)
V: Cell voltage (V)
x_i: Mole fraction of species i

Greek letters

α: Transfer coefficient
ε_p: Electrode porosity
ε_{SOFC}: SOFC electrical efficiency
$\eta_{activation}$: Activation overpotential (V)
$\eta_{concentration}$: Concentration overpotential (V)
η_{ohmic}: Ohmic overpotential (V)
σ_{anode}: Anode conductivity (1/Ω m)
$\sigma_{cathode}$: Cathode conductivity (1/Ω m)
$\sigma_{electrolyte}$: Electrolyte conductivity (1/Ω m)
τ_{anode}: Anode thickness (m)
$\tau_{cathode}$: Cathode thickness (m)
$\tau_{electrolyte}$: Electrolyte thickness (m)
$\tau_{tortuosity}$: Electrode tortuosity